JOIV : Int. J. Inform. Visualization, 9(1) - January 2025 433-438

INTERNATIONAL JOURNAL ON INFORMATICS VISUALIZATION

journal homepage : www.joiv.org/index.php/joiv

Robust and Automatic Algorithm for Palmprint ROI Extraction

Noor A. Yousif [a], Samar Amil Qassir [b,*], Dena Nadir George [b]

[a] Department of Control and Systems Engineering, University of Technology-Iraq, Baghdad, Iraq
[b] Department of Computer Science, College of Science, Mustansiriyah University, Baghdad, Iraq
Corresponding author: *samarqassir@uomustansiriyah.edu.iq

***Abstract*—The ridges, creases, wrinkles, and minutiae on the palmprint region of interest (ROI) are important features. These features are employed to confirm or identify an individual. One inevitable issue in the realization of palmprint recognition systems is the extraction procedure of this region under unrestricted environments. The variety in palm sizes, postures, lighting conditions, and backgrounds, however, certainly presents a significant issue. Finding and extracting the palm's area of interest (ROI) will be our main goal. This research introduces a robust automated algorithm based on square construction and each YCbCr color space features. After reading the image of the colored hand, this algorithm goes through two stages. Firstly, convert to the YCbCr color space. This stage guarantees precise locating of the hand region in addition to deleting irrelevant information from the image. Secondly, determining ROI is based on applying three steps: locating three key references, utilizing these key references to construct the main line, and finally, constructing the ROI square. The total color hand images (230) were used to test and evaluate the newly introduced algorithm; 30 were collected from the internet; and 200 were chosen from the Birjand University Mobile Palmprint Database (BMPD). The hand images include two orientations, left and right, varying sizes and backgrounds, uneven illumination, shadows, and some hand images have items on the finger(s). The experimental findings demonstrate that the introduced algorithm effectively attained 100% and 99.565% sensitivity and accuracy, respectively.**

***Keywords*—Biometric; palmprint detection; YCbCr color space; ROI segmentation.**

Manuscript received 10 Apr. 2024; revised 12 Jun. 2024; accepted 19 Aug. 2024. Date of publication 31 Jan. 2025.

I. INTRODUCTION

An individual can be automatically identified by a biometric identification system using behavioral or physical traits [1], [2], [3]. Because the palmprint offers essential information for personal identity, researchers have recently been more interested in using palmprints for identification [4]. Its range extends from the wrist to the base of the fingers; Fig. 1 illustrates the various hand portions. There are typically three flexion creases, secondary creases, and ridges on the inside surface of the palm. The secondary creases are referred to as wrinkles, while the flexion creases are also known as primary lines. Palmprints vary, even in identical twins [5], [6], [7], [8]. These intricate, non-genetically predictable patterns are highly helpful for identifying individuals. The recognition rate of crease-based identification techniques is equivalent to that of face and fingerprint recognition techniques, suggesting that they are a promising approach [9], [10], [11].

The palmprint region is bigger and hence has more details than the finger. Previous studies have demonstrated that a palmprint-based biometrics system offers a number of unique benefits over an iris-based personal biometrics system, including steady line characteristics, minimal distortion, and simple self-positioning [12]. It can also digest information quickly and attain a high recognition rate. While several researchers have noted the efficacy and use of palmprints for identification, there are not many published studies on enhancing palmprint recognition for individualization. An important stage in such image-based biometric systems is locating and extracting the ROI [13], [14], [15], [16].

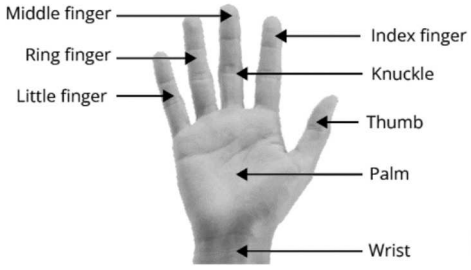

Fig. 1 Different hand sections.

Adjusting the hand images for orientation and scale normalization is the goal of ROI extraction for palmprint identification. The center portion of the normalized hand image is then cropped for the subsequent feature extraction. Given that the quality of the ROI extraction greatly affects the recognition performance, it is obvious that efficient ROI extraction method is essential for palmprint identification. Thus, developing a successful ROI extraction technique is a crucial area of study for palmprint recognition researchers [17].

This research introduces a robust and automatic ROI extraction algorithm to enhance and accelerate the automatic ROI segmentation. This region is approximately 7–11 cm by 7–11 cm and contains all the key creases. The manual extraction of this region is laborious, time consuming, inconsistent, and error prone. The described algorithm's primary contributions are to precisely detect and extract the important ROI from palmprint images, thereby increasing the accuracy and dependability of palmprint identification systems. Using skin color modeling to identify the hand in the image and three primary key references that will be utilized for location, construct the square of ROI.

There are diverse range of research that has been conducted to localize and segment ROI for palmprint recognition systems. Wang et al. [18] presented an automated ROI to achieve high-resolution palmprint identification for forensic purposes, segmentation method based on datum point detection. To get strong edges and gradient magnitudes, a whole palmprint is first subjected to the Canny edge detector. The gradient magnitude picture's convex hull left and right differential images, and strong edge image are then used to identify the initial datum point, or the heart line's endpoint. The position, direction, and statistical average distance between the first and second datum points are used to estimate a second datum point, which is the lifeline's terminus. Lastly, using the two datum points and their perpendicular bisector, segmented palm areas are produced. The accuracy of the presented ROI segmentation approach is compared to manual segmentation using complete palmprint photos from the public high-resolution palmprint database THUPALMLAB. For the interdigital, thinner, and hypothenar areas, the corresponding regional error rates are 15.72%, 17.05%, 21.38% and total error was19.54% respectively.

El et al. [19] the authors of this work propose a method for extracting palm ROI from contactless hand images. The method is based on blob analysis and requires no training or parameter adjustments. It can produce palm ROI, rotation-adjusted hand, hand valley points, and the left or right hand. It can also handle variations in the number of finger holes that may arise from wearing rings or from incorrectly rejecting hand pixels during the hand segmentation step. Three publicly accessible hand DBs are used to methodically test the method: Sfax, IITD, and PolyU 3D/2D. For the three DBs, the technique yields palm extraction errors of 0.27%, 0.26%, and 0%, respectively. The entire technique has been demonstrated to withstand scaling and 360° rotations. After performing extensive scaling and rotation testing, the mean extraction error for the three DBs may rise by no more than 0.9%.

An adaptive ROI segmentation methodology was presented in Zhao and Zhang [20], whereby the palm is identified from the image using a support vector machine-based technique, and a coordinate system is constructed to guarantee the ROI's correctness. The four phases of the suggested method begin with the enhancement of a palmprint image. Niblack-based binarization comes next. After this point, the palm becomes more coarsely binarized than finely binarized. After that, palm detection is carried out using an SVM classifier that separates the palm's foreground and background pixels. The final step involves locating important references to create a coordinate system for finding and extracting the ROI. Tests of the suggested technique were conducted using the extensive hyperspectral palmprint datasets PolyU-Multi and CASIA-Multi, which span 26 spectrum bands at 20 nm intervals from 520 to 1030 nm. The experimental findings demonstrated a 99.51% recognition accuracy and an equal error rate (EER) of 1.49%.

An approach for automatically segmentation palmprint ROI from whole-hand photos using straight line clusters was presented by Xiao et al. [21]. This approach starts by converting the original whole-hand image into a binary image. Then a large number of straight lines were created in accordance with a number of preset guidelines. It is possible to determine that a single straight line crosses four fingers if there are eight places where it intersects with the hand region. The locations of the finger joint sites are clear in this instance. Then, in these finger joint regions, further critical point candidates can be found. Thus, four-finger joint regions may yield a large number of critical point possibilities. Four cluster centers are computed using the k-means clustering technique and are regarded as the last four important references. Additionally, we can determine the order in which the four important references are located by using the distance information between them. A coordinate system can be created using the last set of key references. The hand's core area may be used to extract the ROI in this new coordinate system. 16,000 whole-hand images from a database were used to test the system. The experimental findings show excellent localization and extraction accuracy may be attained with the suggested strategy.

Luo and Zhong [22] introduced a new approach to extracting ROI from palmprint images. Preprocessing was done in order to get rid of the unnecessary background in the first phase. The 14 key points in each image were determined in the second stage, which involved defining a coordinate system based on these points in order to extract the area of interest ROI from the palmprint. To increase the method's accuracy, additional network and data imbalance functionality is included. Using the XJTU-UP palmprint database dataset, the suggested method's effectiveness was confirmed and validated. According to the XJTU-UP database findings, when the false acceptance rate is 0.01% compared to the suboptimal technique, the genuine acceptance rate can be increased by up to 20.56% and the recognition accuracy can rise by a maximum of 2.16%.

In this work, each of the YCbCr color models and the mathematical characteristics of square construction were adapted to develop the introduced algorithm. These approaches are explained as follows.

A. YCbCr Color Space

Another kind of color space that is used to convert images is called YCbCr. It has three channels: The Y-channel, which represents light or the grayscale counterpart of an image, and

the other two channels, which represent the color levels in this space [23]. An image can be represented more effectively by using this color space. In order to color the brightness in a given scene, it first separates the luminance and coloring components and uses fewer components overall. The conversion of RGB to YCbCr is accomplished using the following formulas:

$$Y = 0.299R + 0.587G + 0.114B \quad (1)$$

$$Cb = 128 - 0.168736R - 0.331264G + 0.5B \quad (2)$$

$$Cr = 128 + 0.5R - 0.418688G + 0.081312B \quad (3)$$

For transformation procedures represented by equations (1), (2), and (3), R stands for red, G for green, and B for blue [24]. In the YCbCr color space as shown in Fig. (2), the redundancies in the source RGB image's three-color channels are more effectively suppressed. To simulate improved human eyesight, YCbCr represents the chromaticity (Cb and Cr) and brightness (Y) color spaces. Because the R, G, and B color channels' redundancy has been eliminated, quantization procedures perform better in this color space [25], [26], [27].

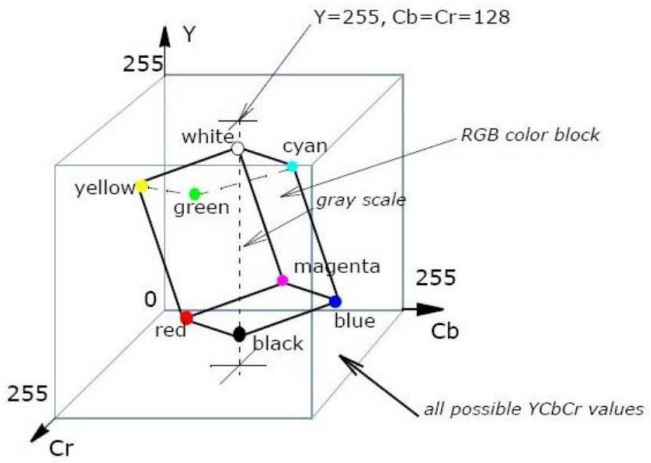

Fig. 2 The YCbCr space [28]

B. The Characteristic of square construction

A square is a four-sided, closed, two-dimensional (2D) shape. A square has four equal sides that are parallel to one another. A ruler and compass can be used to build a square in its simplest form. Fig. 3 illustrates a square's fundamental shape. A rectangle with two adjacent sides of equal length can also be used to describe it. It is the only regular polygon whose diagonals are all the same length and whose internal, exterior, and central angles are all identical (90°) [29].

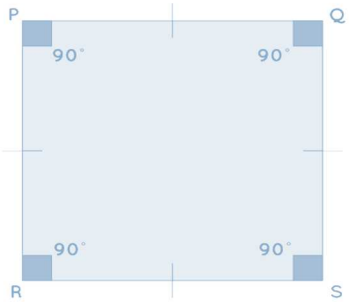

Fig. 3 The Square's fundamental shape and properties [30]

A square has several significant characteristics, including the fact that all internal angles add up to 360° and that a square's diagonals intersect one another at a 90° angle. The diagonals are all the same length, and they are longer than the sides. The square is divided into two congruent triangles by the diagonals [30].

II. Material and Method

The steps of the ROI locating and extracting algorithm are the focus of this section, each stage is illustrated in detail. As well as the diagram of the introduced algorithm is presented as shown in Fig. 4. Using examples that the introduced algorithm tests, the implementation procedures are demonstrated in detail.

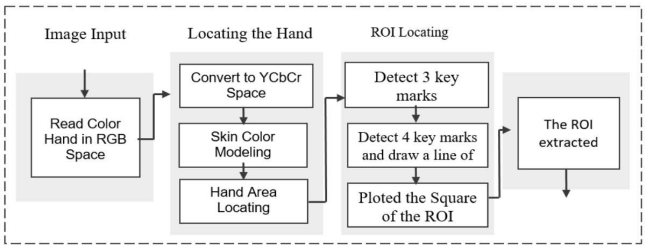

Fig. 4 Diagram of the introduced algorithm's stages

A. Stage 1

The color hand image is entered as a JPEG in an RGB space of size (N×M), where N and M represent the image's rows and columns, respectively.

B. Stage 2

Locating the hand is the objective of this stage. Three steps are involved in it:

1) Conversion to YCbCr color space: the convention used equations illustrated in section III. Fig. (5) shows the result of converting the hand image.

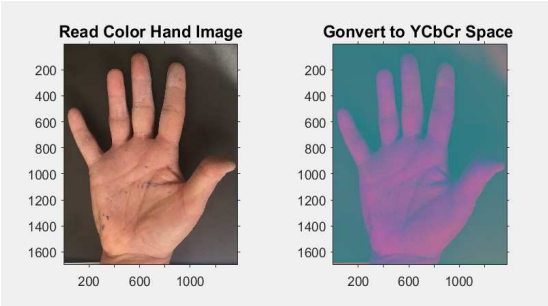

Fig. 5 Convert the color space of the hand image to YCbCr.

2) Segmentation of the hand region: Based on the observation of the YCbCr subspace, which demonstrates strong differentiation in skin color comparing with RGB color space as Histogram Distribution illustrated in Fig. 6 and 7.

The range thresholds for intensity values between (0 and 255) for each of the Y, Cb, and Cr bands are derived; the Y values exhibit the most pronounced split of the skin and non-skin areas. After attempting a wide variety of thresholds and testing a large number of samples; Four boundary constraints were derived as explained in the following equations (4-7).

The skin in band Y has values between 45 and 185, in band Cb between 95 and 110, and in band Cr between 145 and 170.

$$(Y > 45)\ and\ (Y < 185) \quad (4)$$
$$(Cb > 95) and\ (Cb < 110) \quad (5)$$
$$(Cr > 145)\ and\ (Cr < 170) \quad (6)$$
$$(Cr > Cb)\ and\ (Cr - Cb > 16) \quad (7)$$

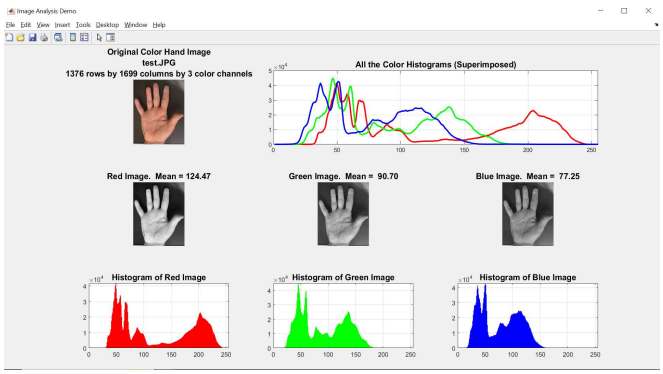

Fig. 6 Hand image histogram distribution in RGB Space

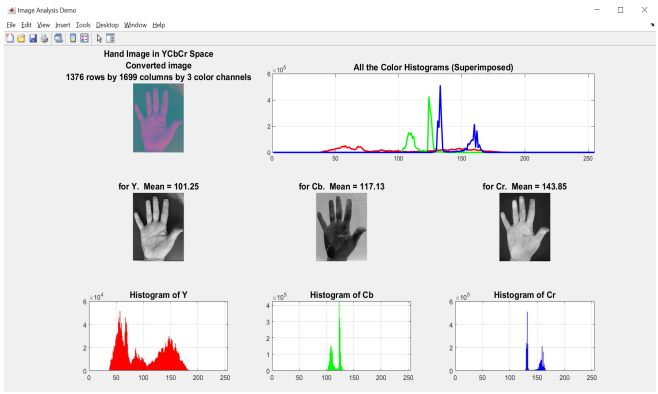

Fig. 7 Hand image histogram distribution in YCbCr space

3) Perform a scan of all the image's pixels: Skin color pixels are identified as those that satisfy equations (4–7) and are assigned a value of 0, while non-skin pixels are fixed at 255. The implementation of this stage shown in Fig. 8.

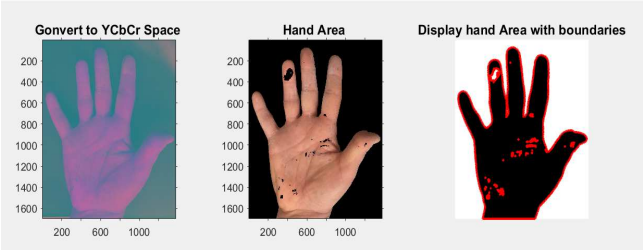

Fig. 8 The implementation of stage 2

C. Stage 3

Locating the square of the ROI is the goal of this stage, which is accomplished by following steps:

1) Key References Locating: The goal of this step is to locate the minimal point from the top by scanning the skin area's coordinates. The minimal value of the y-coordinates, the borders of the skin region with a value of 0, is the first key reference (KR1) in this scanning. As seen in Fig. 9, this minimal y value, which stands for the upper margins, is indicated by a blue point. The other two key references, KR2 and KR3, are identified by a blue point at the initial place on the left and right of the transition from skin pixel to non-skin pixel and vice versa. These two references are recognized on the same finger. In this step, the distance between KR2 and KR3 is calculated.

2) Main Line Construct: As shown in Fig. 9, a straight line is created in this step from the location of KR1 to the mid-distance between KR2 and KR3. This step's goal is to measure one side of the ROI's square in length. This processing is based on the fact that the length of the middle finger (from its beginning to its end) is equal to the length from its end to the wrist area on the hand, which represents the length of the ROI that our aim is to locate and extract.

3) ROI Square Construct: Using the length of line obtained in the second step as a guide, draw the square according to the properties of square construction. This square, which represents the palm ROI, is based on the idea of a geometrical square whose four edges are all the same length, as mentioned in section III. The first side's is drawn based on the line length, where its center matches the mid-distance between the KR2 and KR3. Each of the second and third square's sides is constructed to form the end point of the first line. The final side is drawn parallel to the first side and closed at the end points of sides two and three.

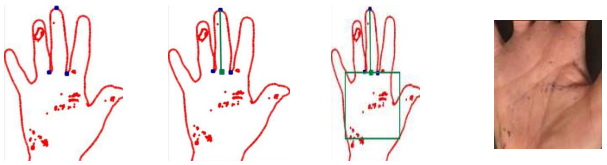

Step1 Key references locating | Step2 Main line construct | Step3 ROI square construct | The outcome of algorithms

Fig. 9 The three steps of locating ROI

III. Result and Discussion

An Intel Core i7 CPU with 8 GB of RAM is used to implement the introduced algorithm, using MATLAB's R2023a version. 30 of 230 contactless color images used in this work were collect from the internet, and the remaining 200 obtained from the Birjand University Mobile Palmprint Database (BMPD), which has 1640 color images of the left and right hands of 41 men and women. The hand image's background varies in color; some are gray, blue, or white, while others are black. The images contained in this database were captured in a free environment, 40–60 cm away from the user's hand. For algorithm evaluation, as shown in equations (8) and (9), the following factors were taken into consideration while determining the accuracy and sensitivity metrics that were used as explained in Table I:

TABLE I
DEFINITION USED IN EVALUATION THE INTRODUCED ALGORITHM

Evaluation metric name	Evaluation Definition
TrueR	represent hand exist with correct ROI located and extracted
TrueNR	represent hand does not exist with no ROI located
FalseR	represent non-hand exist with ROI located and extracted

Evaluation metric name	Evaluation Definition
FalseNR	represent the hand exist with no ROI located

$$\text{Sensitivity} = \frac{(\text{TrueR})}{(\text{TrueR})+(\text{FalseR})} \times 100 \quad (8)$$

$$\text{Accuracy} = \frac{(\text{TrueR})+(\text{TrueNR})}{(\text{TrueR})+(\text{TrueNR})+(\text{FalseR})+(\text{FalseNR})} \times 100 \quad (9)$$

Fig. 10 displays many dataset instances along with their outcomes after using the introduced algorithm. The number of hand images is 230, while for 222 hand images, the ROI was located and extracted correctly. 7 images had no hand, which was correctly identified as such, and 1 image had an incorrect result as having no ROI. The remaining images, zero, indicate non-hand existence with ROI locate and extract, as shown in Table II. Table III explains that the introduced algorithm produces better results than the other works that were compared with them.

TABLE II
THE SENSITIVITY AND ACCURACY OF INTRODUCED ALGORITHM

Total images	TrueR	TrueNR	FalseR	FalseNR	Sensitivity	Accuracy
230	222	7	0	1	100%	99.565%

TABLE III
COMPARISON OF THE INTRODUCED ALGORITHM WITH OTHER WORKS

Related Works	Method	Total Error
Wang et al. [18]	Based on using Canny edge detector	19.54%
El et al. [19]	based on blob analysis and tested by 3 DBs	0.9 %
Zhao and Zhang [20]	support vector machine-based technique, and a coordinate system	1.49 %
Introduced algorithm	Introduced algorithm	1.46 %

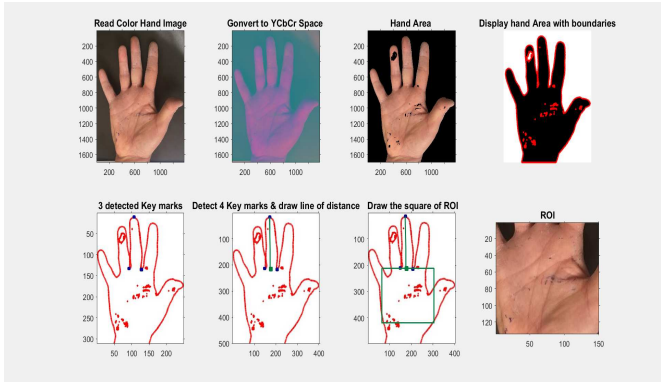

Example 1 Right Orientation and gray background

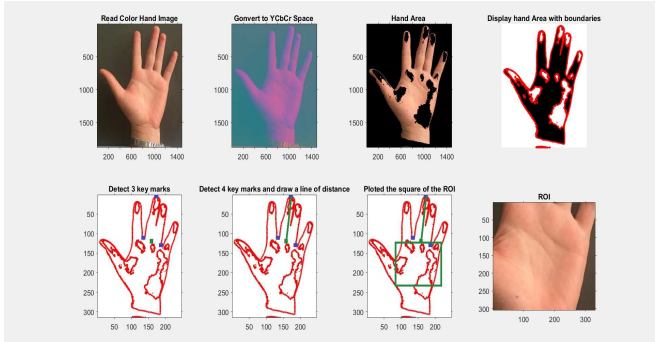

Example 2 Left Orientation and gray background

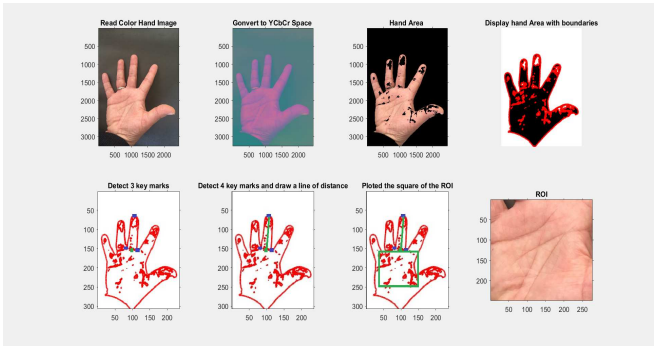

Example 3 Right Orientation and ring on finger

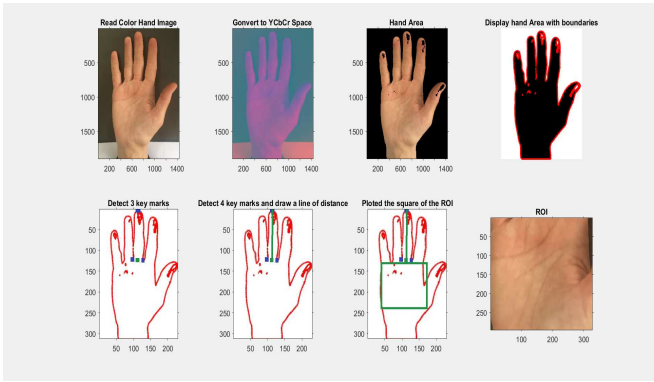

Example 4 Right Orientation and mix color of background

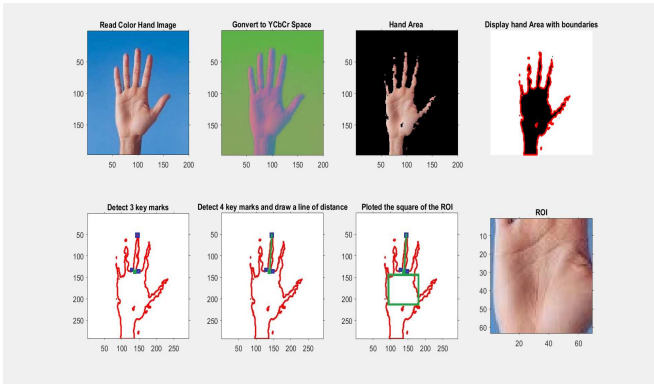

Example 5 Right Orientation and blue background

Fig. 10 Examples of introduced algorithm results

IV. CONCLUSION

A reliable algorithm for locating and extracting the ROI of a palmprint was presented in this research. Using the YCbCr color space, which is essential to guarantee precise hand area detection. After reading the color hand image, the algorithm involves two stages: hand location and ROI locating and extracting. The initial stage relied on color characteristics, demonstrating that the YCbCr color space is a good choice for identifying skin color since it produces high-quality detection outcomes. This stage guarantees precise identification of the hand region in addition to deleting irrelevant information from the image. In the second stage, the segmented hand was bound to make it easier to scan the skin area coordinates and identify the first key reference, which is the least point from the top. The other two key references were detected based on the first reference, and all will be used for line construction, then for ROI square construction. The introduced algorithm achieves accurate ROI segmentation in palmprint images by integrating these approaches.

Specifically, the skin area detection based on YCbCr was able to identify and extract the ROI even in cases where the hand image had items on the finger(s) that varied in size, position, and background, as well as poor contrast, uneven lighting, and shadows. This exhibits resilience and signifies a noteworthy progression that can be used in palmprint recognition systems, enabling more effective feature extraction. For future work, subsequent efforts may involve the extraction of all principal lines and wrinkle characteristics, which can feed them into a machine learning system for biometric identification purposes.

ACKNOWLEDGMENT

The authors of this article express their gratitude to Mustansiriyah University (www.uomustansiriyah.edu.iq) in Baghdad, Iraq, for providing assistance for this work.

REFERENCES

[1] F. E. Sadeq, and Z. T. M. Al-Ta'i, "Comparison Between Face and Gait Human Recognition Using Enhanced Convolutional Neural Network", *Journal of Applied Engineering and Technological Science (*JAETS), 5(1), 18-30, 2023.

[2] A. A. Ismail, A. Babu, E. Barka, and K. Shuaib. "AI-powered biometrics for Internet of Things security: A review and future vision", *Journal of Information Security and Applications,* vol. 82, pp. 103748, May 2024.

[3] S. Abdul-Kader Hussain, H. Al-Nayyef, B. Al Kindy, and S. Amil Qassir, "Human Earprint Detection Based on Ant Colony Algorithm", *Int J Intell Syst Appl Eng*, vol. 11, no. 2, pp. 513–517, Feb. 2023.

[4] J. Khodadoust, R. Monroy, M.A. M.-Pérez, O. L. González, W. Kusakunniran, A. Boller and P. Terhörst. "A novel indexing algorithm for latent palmprints leveraging minutiae and orientation field", Intelligent Systems with Applications, vol. 21, pp. 200320, Mar. 2024.

[5] S. Ma, Q. Hu, S. Zhao, S. Chen, and L. Jiang, "SYEnet: Simple yet effective network for palmprint recognition," *Information sciences*, vol. 669, pp. 120518–120518, May 2024, doi:10.1016/j.ins.2024.120518.

[6] S. Li, L. Fei, B. Zhang, X. Ning, and L. Wu, "Hand-based multimodal biometric fusion: A review," *Information Fusion*, p. 102418, Apr. 2024, doi:10.1016/j.inffus.2024.102418.

[7] H. Wang, L. Su, H. Zeng, P. Chen, R. Liang, and Y. Zhang, "Anti-spoofing study on palm biometric features," *Expert Systems with Applications*, vol. 218, p. 119546, May 2023, doi:10.1016/j.eswa.2023.119546.

[8] L. Su, L. Fei, S. Zhao, J. Wen, J. Zhu, and S. Teng, "Learning modality-invariant binary descriptor for crossing palmprint to palm-vein recognition," *Pattern recognition letters*, vol. 172, pp. 1–7, Aug. 2023, doi:10.1016/j.patrec.2023.05.026.

[9] Ooi Zhi Jie, Lim Tong Ming, and Tan Chi Wee, "Biometric Authentication based on Liveness Detection Using Face Landmarks and Deep Learning Model," *JOIV: International Journal on Informatics Visualization*, vol. 7, no. 3–2, pp. 1057–1065, Nov. 2023, doi:10.30630/joiv.7.3-2.2330.

[10] Ganjar Gingin Tahyudin, Mahmud Dwi Sulistiyo, Muhammad Arzaki, and E. Rachmawati, "Classifying Gender Based on Face Images Using Vision Transformer," *JOIV: International Journal on Informatics Visualization*, vol. 8, no. 1, pp. 18–18, Mar. 2024, doi:10.62527/joiv.8.1.1923.

[11] A. Setiawan, Riyanto Sigit, and Rika Rokhana, "Face Recognition Using Convolution Neural Network Method with Discrete Cosine Transform Image for Login System," *JOIV: International Journal on Informatics Visualization*, vol. 7, no. 2, pp. 502–510, May 2023, doi:10.30630/joiv.7.2.1546.

[12] J. Wan, D. Zhong, and H. Shao, "Palmprint recognition system for mobile device based on circle loss," *Displays*, vol. 73, pp. 102214–102214, Jul. 2022, doi:10.1016/j.displa.2022.102214.

[13] Feng Yulin and A. Kumar, "BEST: Building evidences from scattered templates for accurate contactless palmprint recognition," *Pattern recognition*, vol. 138, pp. 109422–109422, Jun. 2023, doi:10.1016/j.patcog.2023.109422.

[14] G. Ananthi, G. Shenbagalakshmi, A.T. Anisha Shruti, and G. Sandhiya, "Authentication by Palmprint Using Difference of Block Means Code," *Advances in computational intelligence and robotics book series*, pp. 185–199, Jun. 2023, doi:10.4018/978-1-6684-9804-0.ch011.

[15] J. Wan, D. Zhong, and H. Shao, "Palmprint recognition system for mobile device based on circle loss," *Displays*, vol. 73, pp. 102214–102214, Jul. 2022, doi:10.1016/j.displa.2022.102214.

[16] A.-S. Ungureanu, S. Salahuddin, and P. Corcoran, "Toward Unconstrained Palmprint Recognition on Consumer Devices: A Literature Review," *IEEE Access*, vol. 8, pp. 86130–86148, 2020, doi:10.1109/access.2020.2992219.

[17] A. Kong, D. Zhang, and M. Kamel, "A survey of palmprint recognition," *Pattern Recognition*, vol. 42, no. 7, pp. 1408–1418, Jul. 2009, doi:10.1016/j.patcog.2009.01.018.

[18] R. Wang, D. Ramos, J. Fierrez, and R. P. Krish, "Automatic region segmentation for high-resolution palmprint recognition: Towards forensic scenarios," *Biblos-e Archivo (Universidad Autónoma de Madrid)*, Oct. 2013, doi:10.1109/ccst.2013.6922078.

[19] A. S. El, H. M. Ebeid, M. Roushdy, and Z. T. Fayed, "A method for contactless palm ROI extraction," Dec. 2016, doi:10.1109/icces.2016.7821999.

[20] S. Zhao and B. Zhang, "Robust and adaptive algorithm for hyperspectral palmprint region of interest extraction," *IET biometrics*, vol. 8, no. 6, pp. 391–400, Jun. 2019, doi:10.1049/iet-bmt.2018.5051.

[21] Q. Xiao, J. Lu, W. Jia, and X. Liu, "Extracting Palmprint ROI from Whole Hand Image Using Straight Line Clusters," *IEEE Access*, pp. 1–1, 2019, doi:10.1109/access.2019.2918778.

[22] K. Luo and D. Zhong, "Robust and adaptive region of interest extraction for unconstrained palmprint recognition," *Journal of electronic imaging*, vol. 30, no. 03, May 2021, doi:10.1117/1.jei.30.3.033005

[23] Paulo *et al.*, "Efficient machine learning approach for volunteer eye-blink detection in real-time using webcam," *Expert Systems With Applications*, vol. 188, pp. 116073–116073, Feb. 2022, doi:10.1016/j.eswa.2021.116073.

[24] C. Lin, "Face detection in complicated backgrounds and different illumination conditions by using YCbCr color space and neural network," *Pattern Recognition Letters*, vol. 28, no. 16, pp. 2190–2200, Dec. 2007, doi:10.1016/j.patrec.2007.07.003

[25] A. H. Abbas, N. M. Mirza, S. A. Qassir, and L. H. Abbas, "Maize Leaf Images Segmentation Using Color Threshold and K-means Clustering Methods to Identify the Percentage of the Affected Areas," *IOP Conference Series: Materials Science and Engineering*, vol. 745, no. 1, p. 012048, Feb. 2020, doi:10.1088/1757-899x/745/1/012048.

[26] Y.-Z. Bahia, Fedila Meriem, and Bengherabi Messaoud, "Face spoofing detection using Heterogeneous Auto-Similarities of Characteristics," *Engineering applications of artificial intelligence*, vol. 130, pp. 107788–107788, Apr. 2024, doi:10.1016/j.engappai.2023.107788.

[27] Arpita Panigrahi, H. Sharma, and A. Mukherjee, "Video-based HR measurement using adaptive facial regions with multiple color spaces," *Biocybernetics and Biomedical Engineering*, vol. 44, no. 1, pp. 68–82, Jan. 2024, doi:10.1016/j.bbe.2023.12.001.

[28] Nouha Khediri, Mohamed Ben Ammar, and Monji Kherallah, "Comparison of Image Segmentation using Different Color Spaces," *2021 IEEE 21st International Conference on Communication Technology (ICCT)*, Oct. 2021, doi:10.1109/icct52962.2021.9658094

[29] L.-C. Wang, W.-L. Song, and X. Guo, "Out-of-plane compressive mechanical properties of square-twist origami folded-stable state," *International journal of mechanical sciences*, vol. 246, pp. 108104–108104, May 2023, doi:10.1016/j.ijmecsci.2023.108104.

[30] A.-P. Buta, Andrei-Marius Silaghi, Aldo De Sabata, and Ladislau Matekovits, "Multiple-Notch Frequency Selective Surface for Automotive Applications," Jun. 2020, doi:10.1109/comm48946.2020.9142001.